

A Parameter-Efficient Tuning Framework for Language-guided Object Grounding and Robot Grasping

Houjian Yu¹, Mingan Li¹, Alireza Rezazadeh¹, Yang Yang², and Changhyun Choi¹

Abstract—The language-guided robot grasping task requires a robot agent to integrate multimodal information from both visual and linguistic inputs to predict actions for target-driven grasping. While recent approaches utilizing Multimodal Large Language Models (MLLMs) have shown promising results, their extensive computation and data demands limit the feasibility of local deployment and customization. To address this, we propose a novel CLIP-based [1] multimodal parameter-efficient tuning (PET) framework designed for three language-guided object grounding and grasping tasks: (1) Referring Expression Segmentation (RES), (2) Referring Grasp Synthesis (RGS), and (3) Referring Grasp Affordance (RGA). Our approach introduces two key innovations: a bi-directional vision-language adapter that aligns multimodal inputs for pixel-level language understanding and a depth fusion branch that incorporates geometric cues to facilitate robot grasping predictions. Experiment results demonstrate superior performance in the RES object grounding task compared with existing CLIP-based full-model tuning or PET approaches. In the RGS and RGA tasks, our model not only effectively interprets object attributes based on simple language descriptions but also shows strong potential for comprehending complex spatial reasoning scenarios, such as multiple identical objects present in the workspace. Project page: <https://z.umn.edu/etog-etrg>

I. INTRODUCTION

Target-oriented grasping is a critical yet challenging task in robot manipulation, requiring both precise object identification and high grasping accuracy to retrieve the correct target. To address this, researchers have developed image-driven methods [2], [3], [4], [5], [6], where the robot receives a reference image of the target object, localizes it using object recognition or matching models [7], [8], [9], [10], and predicts grasp poses based on detection bounding boxes or segmentation masks. However, object grounding performance degrades when the reference image differs from the target in the workspace due to factors like lighting, viewpoint, or occlusion. Another approach focuses on language-guided robot grasping [11], [12], [13], [14], [15]. While language inputs offer greater flexibility than images, they can introduce ambiguity if not carefully articulated. For instance, as shown in Fig. 1c, if the input is “mustard bottle” and multiple instances are present, the robot may struggle to grasp the correct one. More detailed linguistic descriptions (e.g., “The Mustard Bottle that is to the upper right of the workspace” in Fig. 1c) reduce ambiguity but

*This work was supported in part by the Sony Research Award Program and NSF Award 2143730.

¹ The authors are with the Department of Electrical and Computer Engineering, Univ. of Minnesota, Minneapolis, USA {yu000487, li002852, rezaz003, cchoi}@umn.edu

² Yang Yang is with the Department of Computer Science and Engineering, Univ. of Minnesota, Minneapolis, USA yang5276@umn.edu

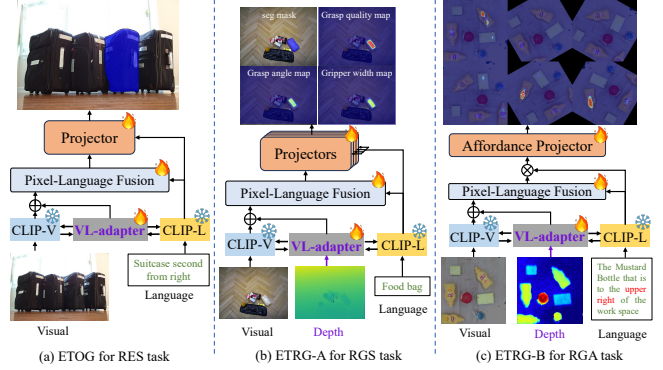


Fig. 1: **Efficient-Tuning pipeline for language-guided object grounding and robot grasping tasks.** We propose Efficient-Tuning Object Grounding (ETOG) for RES task, Efficient-Tuning Robot Grasping type-A (ETRG-A) for RGS task, and type-B (ETRG-B) for RGA task. Our framework with minor modifications is able to solve the three tasks. *Zoom-in for more details.*

increase the complexity of vision-language comprehension. Previous works primarily focus on interpreting simplified language expressions [12], using basic colors and shapes [13], or selecting a distinct target without duplicates [12], [14]. To address these limitations, an ideal language-guided grasping pipeline should: (1) handle open-vocabulary inputs, (2) interpret complex language descriptions to resolve object ambiguities, and (3) accurately localize and grasp the target with high success rates.

Recent robot grasping studies using Large Language Models (LLMs) or Multimodal Large Language Models (MLLMs) have demonstrated strong object grounding and grasp detection performance [16], [17], [18], [19], [20]. However, full-model training or fine-tuning is computationally expensive and may suffer from catastrophic forgetting [21], limiting the feasibility of local deployment. In this paper, we propose a parameter-efficient tuning (PET) approach [22], [23] for object grounding and robot grasping, enabling competitive performance by incorporate a lightweight module into a frozen pre-trained model. Specifically, we propose a CLIP-based PET framework for object grounding and robot grasping. As shown in Fig. 1, our framework, with minor modifications on the task projector, addresses three challenging vision-language tasks: Referring Expression Segmentation (RES) [24], Referring Grasp Synthesis (RGS) [11], [16], and Referring Grasp Affordance (RGA) (see Section III-A) for which the framework processes visual images and complex linguistic descriptions to predict object segmentation masks, grasp-related maps, and grasp affordance maps, respectively.

Our primary contributions are as follows: (1) We propose a bi-directional vision-language adapter that fuses features from multiple modalities and enhances the cross-modal interaction for pixel-level language understanding. By fine-tuning the lightweight adapters (only 0.8% to 2.0% of the frozen CLIP backbone parameters) along with the task decoder, we achieve performance comparable to full-model fine-tuning baselines. (2) We introduce a depth fusion branch that integrates geometric cues with vision and language features, improving 4-DoF grasp pose predictions. (3) We present **Efficient-Tuning for Object Grounding (ETOG)** and **Efficient-Tuning for Robot Grasping type-A (ETRG-A)** and type-B (**ETRG-B**) models for three key vision-language tasks, with minor modifications to our framework. Extensive evaluations demonstrate the effectiveness of our design in handling open-vocabulary language inputs and complex spatial reasoning. Each model is trained end-to-end, with the only prior knowledge being the pre-trained CLIP model [1].

II. RELATED WORKS

A. Language-guided Object Grounding

The object grounding task aims to localize the target instance described by a language expression. Based on the output format (bounding boxes or segmentation masks), it can be categorized as referring expression comprehension (REC) or referring expression segmentation (RES). Our proposed method focuses on pixel-level vision-language alignment and mask predictions, primarily designed for the RES task. CLIP-based RES methods leverage the strong text-image alignment of the CLIP model [1], typically combining the CLIP backbone with a multimodal decoder for cross-modal interactions [22], [23], [25], [26], [27]. Most of these methods use full-model fine-tuning and are limited to the RES task. In contrast, our approach emphasizes parameter-efficient tuning and extends object grounding into robotics tasks.

B. Language-guided Robot Grasping

Recent advances in multimodal learning have enabled robots to understand human language instructions and generate accurate grasp pose [11], [12], [16], [18], [20], [28], [29]. Language-guided grasping typically involves two stages: first, obtaining a target object’s bounding box or segmentation mask, then feeding it into a grasping pipeline [28], [30], [25]. Some researchers have explored end-to-end approaches for generating grasp poses in Referring Grasp Synthesis (RGS) [11], [29], while others have focused on predicting grasp poses via affordance maps in Referring Grasp Affordance (RGA) [12], [31], bypassing the need for object bounding boxes or segmentation masks. Our work addresses both tasks simultaneously within an efficient-tuning framework.

C. Parameter-Efficient Tuning

Traditional fine-tuning updates all model parameters to adapt to a new task, but as models grow larger, this becomes computationally expensive. Parameter-efficient tuning (PET)

methods—such as adapters [32], [33], [34], prefix-tuning [35], LoRA [36], and prompt-tuning [37]—address this by updating only a small subset of parameters or adding task-specific parameters, while keeping most pre-trained parameters unchanged. These methods reduce memory usage, accelerate training, and facilitate efficient transfer learning, making it easier for roboticists to adapt large pre-trained foundation models to new tasks with lower computational demands. Recent works [22], [23] focus on object grounding, while our approach combines both object grounding and grasping tasks. Additionally, we introduce a novel method to integrate depth information into the RGB-only pipeline, improving robot grasp predictions.

III. METHODS

In this section, we propose a parameter-efficient tuning (PET) framework for language-guided object grounding and robot grasping.

A. Problem Formulation

As shown in Fig. 1, we provide detailed formulations for the following three tasks. We use $I \in \mathbb{R}^{H \times W \times 3}$ to represent image input where (H, W) denote the image resolution, $T \in \mathbb{R}^L$ for a language expression, and $D \in \mathbb{R}^{H \times W}$ for a depth image. Our pipeline takes visual images and language descriptions as inputs and outputs task specific predictions as follows. **RES Task:** We follow the classical RES definition [24] for this task. Given an image I and a language expression T describing specific parts of the image, the model is tasked to segment the corresponding area(s) of the language description obtaining a segmentation mask $M \in \{0, 1\}^{H \times W}$. We refer this task as object grounding. **RGS Task:** Given an RGB image I , a depth image D and a language expression T referring a unique object in the image, the goal is to predict a segmentation mask of the target object on which 4-DoF grasp poses $G = \{x, y, \theta, l\}$ (a.k.a grasp rectangles) are hypothesized. Here, (x, y) denotes the gripper center location at the image coordinate, θ indicates the gripper rotation at the camera frame, and l indicates the gripper open width. Following [11], the model predicts three maps to recover the gripper pose G . More specifically, (x, y) is determined by the max value’s pixel coordinate in grasp quality map Q . The rotation angle is provided by $\theta = \Theta(x, y)$ where Θ is the grasp angle map. Similarly the gripper open width map P produces $l = P(x, y)$. **RGA Task:** Given an RGB image I , a depth image D , and a language expression T referring a target object in the scene, the goal is to grasp the target object based on the predicted pixel-wise grasp affordance maps with N different rotation angles $Q_g \in \mathbb{R}^{H \times W \times N}$ [12]. We also employ a 4-DoF grasp pose $G = \{x^*, y^*, \theta^*, z\}$ to represent the grasping motion, where $(x^*, y^*, \theta^*) = \operatorname{argmax}_{(x, y, \theta)} Q_g(x, y, \theta)$ and $z = D(x^*, y^*)$.

B. Multimodal Feature Early Fusion

The framework details are shown in Fig. 2. The model inputs consist of RGB images I , language expressions T ,

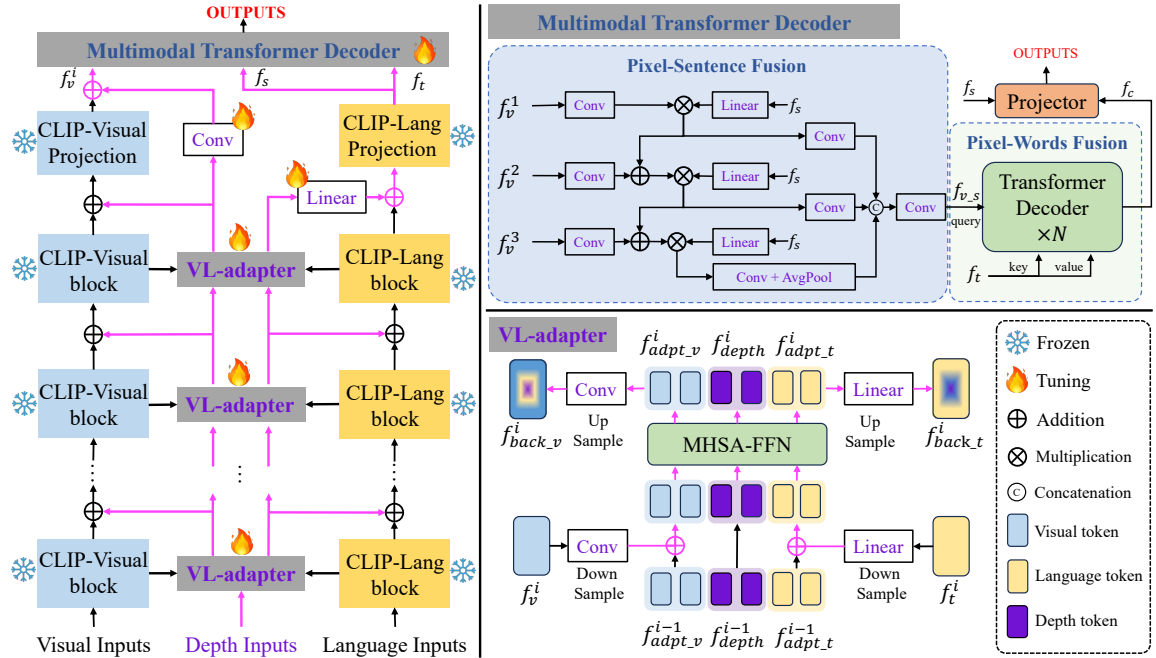


Fig. 2: Our model takes visual, language and depth (optional, depending on tasks) as inputs and outputs the task predictions. Our VL-adapter fuses the multimodal features extracted from CLIP at different stages and previous VL-adapter layers. The Pixel-Sentence Fusion module combines multi-scale visual features with a sentence-level global representation, while the Pixel-Words Fusion module focuses on word-level token understanding and eventually generates the segmentation masks.

and optional inputs from a different modality (e.g. depth images D) depending on the task type. The frozen CLIP image encoder and text encoder extract i -th early-stage visual and language intermediate features $f_v^i \in \mathbb{R}^{H_i \times W_i \times C_i}$ and $f_t^i \in \mathbb{R}^{L \times C_t}$, where H_i, W_i, C_i are the height, width and number of channels of f_v^i respectively, L is the language token length, C_t is the number of channels of the language token, $i \in \{1, 2, \dots, N\}$, and N denotes the number of CLIP vision ResNet [38] or vision Transformer (ViT) [39] blocks based on the choice of CLIP backbones.

To enhance cross-modal feature interaction between the originally separated vision and language encoders, we propose our novel VL-adapter to execute vision-language feature early fusion. Before feeding the vision f_v^i and language features f_t^i from previous layers to the next CLIP visual block ϕ_i and language block ψ_i , $i \in \{2, \dots, N\}$, our VL-adapter takes them as input and outputs the refined multimodal features to the corresponding CLIP branch.

In VL-adapter, we first adjust the f_v^i and f_t^i to have the same feature dimension by passing each of them to a convolution layer and a linear layer, respectively. Then, the downsampled visual and linguistic features are added with $f_{adpt_v}^{i-1}$ and $f_{adpt_t}^{i-1}$ passed from the former VL-adapter $\hat{f}_v^i = \text{Conv}(f_v^i) + f_{adpt_v}^{i-1}$, $\hat{f}_t^i = \text{Linear}(f_t^i) + f_{adpt_t}^{i-1}$ where $\text{Conv}(\cdot)$ and $\text{Linear}(\cdot)$ denote convolution and linear layers, respectively. Such an operation reduces computation complexity meanwhile makes sure that the features obtained from the previous stage are able to get to the deeper layers.

Moreover, we concatenate the visual, linguistic, and the optional input feature (e.g., depth feature) from a different modality. For RES task, it only requires visual and linguistic

features. The concatenated tokens are then fed into a transformer layer [40] using the following equation:

$$\begin{aligned} f_{vdt} &= \text{Concat}(\text{LN}(\hat{f}_v^i), \text{LN}(f_{depth}^{i-1}), \text{LN}(\hat{f}_t^i)) \\ f'_{vdt} &= \text{MHSA}(f_{vdt}) + f_{vdt} \\ f''_{vdt} &= \text{FFN}(f'_{vdt}) + f'_{vdt} \\ [f_{adpt_v}^i, f_{depth}^i, f_{adpt_t}^i] &= \text{Split}(f''_{vdt}) \end{aligned} \quad (1)$$

where $\text{Concat}(\cdot)$, $\text{LN}(\cdot)$, $\text{MHSA}(\cdot)$, $\text{FFN}(\cdot)$, and $\text{Split}(\cdot)$ represent concatenation operation, layer normalization, multi-head self-attention layer, feed-forward network, and split operation, respectively. In addition, our VL-adapter outputs the multimodal fused features back to CLIP vision and language branches updating f_v^i and f_t^i : $f_v^i = f_{back_v}^i + f_v^i$ where $f_{back_v}^i = \text{Conv}(f_{adpt_v}^i)$ and $f_t^i = f_{back_t}^i + f_t^i$ where $f_{back_t}^i = \text{Linear}(f_{adpt_t}^i)$.

Unlike the previous in-CLIP design [22] where the fused features did not directly forward outside of CLIP model, we add two stand-alone convolution layer and linear layer (as shown on the left side of Fig. 2) to make sure that the VL-adapter fused information is able to engage in feature interaction at deep layers. This simple but effective modification helps the object grounding task (see Section IV-A). In this case, CLIP model together with VL-adapter will provide visual features f_v^i at multiple stages, sentence-level feature $f_s \in \mathbb{R}^{C_s}$ and word-level feature $f_t \in \mathbb{R}^{L \times C_t}$ where C_s and C_t are the feature dimensions.

C. Multimodal Transformer Decoder

Pixel-Sentence Fusion: We propose a pixel-sentence fusion module to learn sentence-level vision-language features (Fig. 2). Given visual features f_v^i extracted at different stages from

the CLIP visual branch and the sentence feature f_s , we fuse such multi-scale visual features and sentence representations to obtain pixel-sentence multimodal feature $f_{v,s}$. Element-wise multiplication and addition operations are applied to this fusion module.

Pixel-Words Fusion: As shown in Fig. 2, the pixel-words fusion module takes the pixel-sentence feature $f_{v,s}$ and the word-level feature from CLIP model as inputs and executes cross-modal feature interactions in a transformer architecture. Each transformer decoder layer consists of a multi-head self-attention layer, a multi-head cross-attention layer, and a feed-forward network layer. To begin with, the model computes self-attention on the pixel-sentence feature $f_{v,s}$: $f'_v = \text{LN}(\text{MHSA}(f_{v,s}) + f_{v,s})$. We apply post layer normalization through this transformer decoder. Then, we adopt cross-attention to the evolved visual feature f'_v : $f'_v = \text{LN}(\text{MHCA}(f'_v, f_t) + f'_v)$, $f_c = \text{LN}(\text{FFN}(f'_v) + f'_v)$ where $\text{MHCA}(\cdot)$ indicates cross-modal attention. Through such a process, we obtain the multimodal feature f_c which combines multi-scale information from different modalities.

D. Projectors and Training Objectives

Projectors in ETOG and ETRG-A consist of standard convolution and linear layers. They transfer f_c and f_s into $F_c \in \mathbb{R}^{N \times D}$ where $N = \frac{H}{4} \times \frac{W}{4}$ and $F_s \in \mathbb{R}^C$ where $C = K \times K \times D + 1$, respectively. K denotes a customized kernel size and F_s serves as a convolution kernel to operate computation with F_c feature map. We employ a text-to-pixel contrastive loss following [26] to train the object segmentation projectors. The training loss L_{tp} can be formulated as follows: $L_{\text{tp}}(F_t, F_c) = \frac{1}{|\mathcal{P} \cup \mathcal{N}|} \sum_{i \in \mathcal{P} \cup \mathcal{N}} L_{\text{contrast}}^i(F_s, F_c^i)$ where \mathcal{P} and \mathcal{N} denotes the class of 1 and 0, respectively, and $L_{\text{contrast}}^i(F_s, F_c^i) = -\log(\sigma(F_s \cdot F_c^i))$ if $i \in \mathcal{P}$ or $-\log(1 - \sigma(F_s \cdot F_c^i))$ if $i \in \mathcal{N}$ where σ represents the sigmoid function.

Besides L_{tp} , we duplicate the segmentation head three times to supervise the grasp quality maps, grasp angle maps, and gripper open width maps predictions using smooth L1 loss for the RGS task.

For the RGA task, ETRG-B uses the fully convolutional network to decode the multimodal feature for the affordance maps Q_g prediction. To represent grasp pose with different angles, we rotate the vision-language feature F_a , derived from element-wise multiplication of f_s and f_c , by $N = 6$ (i.e., multiples of $\theta = 30^\circ$) orientations predicting pixel-wise scores of horizontal grasps within the rotated maps. Since this task does not require object grounding but directly chooses the pixel with the highest score among all the N maps, we further employ the motion loss $\mathcal{L}_{\text{grasp}}$ from our previous work [12].

IV. EXPERIMENTS

In this section, we conduct language-guided object grounding and robot grasping experiments to evaluate the proposed method. The experiment goals are to verify if: 1) our Efficient-Tuning for Object Grounding (ETOG) generic model is able to correctly ground the target object, 2)

the proposed depth fusion branch in Efficient-Tuning for Robot Grasping (ETRG-A) can contribute to more accurate grasping prediction, and 3) the ETRG-B model manages to understand object-attribute descriptions and achieve high grasping success rate with more complex spatial relationship language inputs. All our models are trained and tested on a workstation with a single NVIDIA RTX 2080 Ti.

A. Referring Expression Segmentation for Object Grounding

RES Datasets: we evaluate our ETOG generic method on three standard RES benchmark datasets: RefCOCO [47], RefCOCO+ [47], and RefCOCOG [48], [49] that include 19,994, 19,992, and 26,771 RGB images, with 142,209, 141,564, and 104,560 annotated language expressions, referring to 50,000, 49,856, and 54,822 annotated objects, respectively. RefCOCO+ is designed to be more challenging by excluding the absolute spatial location description, and RefCOCOG dataset has an average of 8.4 words length in the language descriptions

Evaluation Metrics: We adopt the mean intersection of union (mIoU), overall intersection of union (oIoU), and $\text{Prec}@X$ to verify the object grounding effectiveness. The $\text{Prec}@X$ evaluates the percentage of test results with an IoU value higher than $X \in \{0.5, 0.7, 0.9\}$.

Implementation Details: We train ETOG for 50 epochs with a batch size 16 using the Adam optimizer with an initial learning rate of $5e-5$. The learning rate is decreased with a decay factor of 0.1 at the 35^{th} epoch.

ETOG Comparison with RES Baselines: In Table I, we compare our ETOG with the state-of-the-art CLIP-based RES methods on RefCOCO datasets using mIoU metric. ETOG outperforms all baseline methods across different backbone architectures. CLIPORT-semantic, a variant of CLIPORT [31], excludes the depth processing branch and uses simple element-wise multiplication to fuse vision and language features. The comparison between CLIPORT-semantic and our method highlights the effectiveness of our VL-adapter. In particular, with the CLIP [1] ResNet-101 [38] backbone, our method—using only 1.9M tunable parameters—achieves a 2.66% and 1.95% performance gain across 8 evaluation tasks compared to CRIS [26] and EAVL [27] that are fully CLIP fine-tuned methods. Additionally, ETOG with 1.21M tunable ViT-B-16 backbone parameters shows a 4.35% and 0.73% performance improvement compared to the latest parameter-efficient tuning approaches, ETRIS [22] and BARLERIA [23], respectively. Table II further compares our model with full fine-tuned RES models, showing that ETOG achieves competitive object grounding performance even against non-CLIP-based approaches. Fig. 3 provides qualitative results, including model predictions and feature map visualizations, with the fourth column showing the attention regions of the well-fused multimodal feature f_c . **ETOG Ablation Study.** An ablation study of our VL-adapter can be found in Table III. To make a fair comparison, we only replace our VL-adapter with the corresponding baselines' vision-language fusion modules. It is noticeable that our proposed VL-adapter which combines the vision language

TABLE I: Performance comparison of different SOTA CLIP-based models on RefCOCO related datasets using mIoU metric. Backbone: visual encoder architecture. U: the UMD test split for RefCOCO(g). Params: total number of parameters to be tuned.

Baselines	Conference	Backbone	RefCOCO			RefCOCO+			RefCOCO(g)		AVG	Params
			val	testA	testB	val	testA	testB	val(U)	test(U)		
CLIPORT-semantic [31]	CORL21	CLIP-R50	57.02	61.56	49.16	43.25	51.29	31.99	42.20	43.39	47.48	51.82M
CRIS [26]	CVPR22	CLIP-R50	69.52	72.72	64.70	61.39	67.10	52.48	59.35	59.39	63.33	146.85M
DyCRIS-M [25]	IROS23	CLIP-R50	70.54	73.13	65.63	62.28	67.61	53.25	60.80	60.87	64.26	146.85M
ETRIS [22]	ICCV23	CLIP-R50	70.39	73.11	66.38	60.47	67.11	50.73	59.71	59.95	63.48	25.66M
ETOG (Ours)	ICRA25	CLIP-R50	72.31	75.49	66.62	63.26	69.46	53.27	60.80	61.98	65.40	32.93M
CRIS	CVPR22	CLIP-R101	70.47	73.18	66.10	62.27	68.08	53.68	59.87	60.36	64.25	161.25M
ETRIS	ICCV23	CLIP-R101	71.06	74.11	66.66	62.23	68.51	52.79	60.28	60.42	64.51	25.92M
EAVL [27]	Arxiv23	CLIP-R101	70.65	73.81	66.62	63.42	68.26	54.71	60.93	61.24	64.96	-
ETOG (Ours)	ICRA25	CLIP-R101	73.37	76.16	68.54	64.70	70.86	54.94	63.06	63.66	66.91	30.57M
ETRIS	ICCV23	CLIP-ViT-B	70.51	73.51	66.63	60.1	66.89	50.17	59.82	59.91	63.44	25.37M
EAVL	Arxiv23	CLIP-ViT-B	71.74	74.38	67.24	64.05	68.41	56.82	61.87	62.21	65.84	-
BARLERIA [23]	ICLR24	CLIP-ViT-B	72.40	75.90	68.30	65.00	70.80	56.90	63.40	63.80	67.06	-
ETOG (Ours)	ICRA25	CLIP-ViT-B	73.37	76.90	69.34	65.95	71.47	56.94	63.75	64.63	67.79	29.89M

TABLE II: Comparison on full model fine-tuning RES methods with RefCOCO related datasets using oIoU metric. Backbone: visual encoder architecture. U: the UMD test split for RefCOCO(g) dataset.

Baselines	Conference	Backbone	RefCOCO			RefCOCO+			RefCOCO(g)		AVG
			val	testA	testB	val	testA	testB	val(U)	test(U)	
PCAN [41]	Arxiv22	ResNet-50	69.51	71.64	64.18	58.25	63.68	48.89	59.98	60.80	62.12
VLT [42]	ICCV21	DarkNet-53	65.65	68.29	62.73	55.50	59.20	49.36	52.99	56.65	58.80
MATTNET [43]	CVPR18	ResNet-101	56.51	62.37	51.70	46.67	52.39	40.08	47.64	48.61	50.75
CGAN [44]	ACM20	ResNet-101	64.86	68.04	62.07	51.03	55.51	44.06	51.01	51.69	56.03
DMMI [45]	ICCV23	ResNet-101	68.56	71.25	63.16	57.90	62.31	50.27	59.02	59.24	61.46
ReSTR [46]	CVPR22	ViT-B	67.22	69.30	64.45	55.78	60.44	48.27	54.48	-	59.99
ETOG (Ours)	ICRA25	ResNet50	70.11	73.97	63.76	58.63	65.66	47.86	57.35	59.87	62.15
ETOG (Ours)	ICRA25	ResNet101	71.11	74.30	65.61	60.00	67.27	49.73	60.09	61.23	63.67
ETOG (Ours)	ICRA25	ViT-B	71.35	76.14	66.73	62.33	68.52	51.90	61.12	62.85	65.12

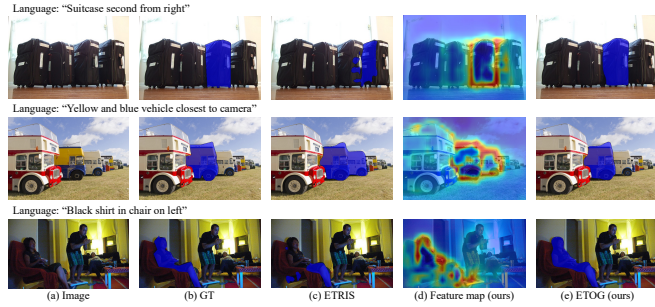


Fig. 3: **Qualitative results on model prediction and feature visualization.** Zoom-in for more details.

tokens and execute multimodal self-attention obtains better mIoU performance compared with previous SOTA vision-language fusion solutions such as parameter-efficient tuning ETRIS’s Bridger [22] and LAVT’s Pixel-Words Attention Module (PWAM) [50]. We also notice that simply adding forward layers (the stand-alone convolution and linear layers shown in Fig. 2) boosts the object grounding performance. In this case, the updated fusion features are forwarded outside of CLIP model and participate the multimodal feature interaction at the deeper layers.

B. Referring Grasp Synthesis with Depth Fusion

RGS Dataset: We evaluate **ETRG-A** on OCID-VLG [11] dataset. OCID-VLG dataset presents a collection of indoor tabletop objects scenes with human annotated image-text-masks-grasp box tuples for referring object grounding and grasp pose prediction tasks. This dataset includes 1,763 scenes with 58 unique object instances and over 89.6k language expressions which contain multiple types of instance-level descriptions.

TABLE III: **ETOG** VL-adapter ablation study. Our proposed VL-adapter with the Forward Layers (FL) achieves the best performance. The following baselines are evaluated on RefCOCO validation dataset with CLIP-R50 backbone. (*) denotes that we re-implement the baseline with its default setup.

Baselines	mIoU	Pr@50	Pr@70	Pr@90
ETRIS* [22]	69.60	81.87	69.53	16.00
LAVT-PWAM [50]	71.25	82.21	70.83	24.66
VL-adapter (Ours)	71.74	82.95	71.49	24.83
VL-adapter+FL (Ours)	72.31	83.22	72.95	26.17

Evaluation Metrics: We report mean intersection of union (mIoU) for the referring object grounding task in the object segmentation format. For object grasping prediction, we apply the Jacquard Index $J@N$ metric [11], [51] measuring the top- N grasp rectangle candidates that have a rotation angle difference less than 30° and IoU over 0.25 compared with the ground truth grasp rectangle.

Implementation Details: We train ETRG-A for 40 epochs with a batch size 11. We adopt the AdamW optimizer with an initial learning rate of $\lambda = 0.0001$ and a polynomial learning rate decay. The images are resized to 416×416 resolution, and the maximum sentence length is set to 20.

Ablation Study on Depth Fusion Branch: One primary SOTA baseline we evaluate against is CROG [11], a CLIP-based RGS method with full model fine-tuned with OCID-VLG dataset. As shown in Table IV, ETRG-A without depth model (ResNet-50) achieves a slightly better (+3.96% $J@1$) performance and competitive object grounding (RES) performance compared CROG. After integrating depth inputs into VL-adapter (details in Fig. 2) fusing the object geometric information into visual-language branches, our ETRG-A with depth fusion full model attains higher grasping rectangle prediction (+11.86% $J@1$) accuracy with ResNet-50 backbone

TABLE IV: **ETRG-A** ablation study. Our proposed depth fusion branch improves the grasping rectangle prediction performance.

Baselines	Backbone	RES	RGS	
		mIoU	J@1	J@Any
CROG	ResNet-50	81.10	77.20	87.70
ETRG-A w/o depth (Ours)	ResNet-50	79.06	81.16	89.11
ETRG-A (Ours)	ResNet-50	79.82	89.06	92.17
ETRG-A w/o depth (Ours)	ResNet-101	79.47	82.28	91.12
ETRG-A (Ours)	ResNet-101	80.11	89.38	93.49

and (+12.18% $J@1$) accuracy with ResNet-101 backbone compared with CROG. CROG is marginally better than our models in the RES task, but we attribute this to the simplicity of the OCID-VLG dataset, which primarily features tabletop objects and lacks the scene diversity found in RefCOCO-related datasets. This environment favors full model fine-tuning methods like CROG, potentially leading to overfitting. Although CROG has 147M tunable parameters which is 3 times larger than our proposed depth-fusion approach, our ETRA-A model still achieves competitive performance on this RES task.

C. Referring Grasp Affordance for Spatial Reasoning

The proposed ETRG-B model is trained using self-supervision in the CoppeliaSim simulator [52]. The primary goal of this RGA experiment is to validate the model’s spatial reasoning capabilities as a beneficial byproduct.

Data Collection: We generate scenes with seven objects, randomly sampled from 32 complex objects, primarily from YCB objects [53]. Ground truth labels are generated using language descriptions based on object attributes, such as color, shape, category name, and spatial location. We employ several language templates to describe both the **Absolute** (target object’s relation to the workspace) and **Relative** (target object’s relation to other reference objects) spatial relationships. The robot agent either randomly selects a target object or employs ETRG-B affordance maps for grasping. Object relabeling is applied if an incorrect object is grasped. For model training, we collected more than 20,000 visual-language-grasp triplets using domain randomization. For testing, 1,600 test cases were generated across the 32 objects, with pre-selected query language descriptions based on target object’s spatial location. All baselines were tested on the same scenes and language expressions.

Implementation Details: We apply online training during the data collection process. Afterward, the entire dataset is replayed for 40 epochs with a batch size of 32. We adopt the AdamW optimizer, with an initial learning rate of $5e-5$ and a polynomial learning rate decay.

TABLE V: **ETRG-B** grasp success rate in simulation. This experiment is designed for model ablation study on spatial reasoning in simulation. We employ CLIP-R50 backbone.

Baselines	Absolute		Relative	AVG
	4-obj	7-obj	7-obj	
ETRG-B w/o depth (Ours)	87.81	86.25	86.18	86.75
ETRG-B (Ours)	90.75	88.38	86.56	88.56

Simulation Results: We evaluate our methods on affordance prediction with spatial reasoning. The experiments include two primary scene types: **Absolute** and **Relative**. In each

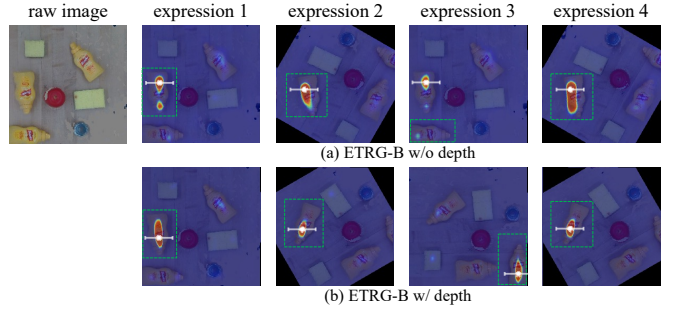


Fig. 4: **Qualitative results on grasp affordance prediction with ETRG-B.** The green bounding boxes highlight the language-referred target. The language expressions used are: (1) “The Mustard Bottle that is to the middle left of the workspace”, (2) “Yellow Mustard Bottle that is to the upper right of the workspace”, (3) “lower left Mustard Bottle” and (4) “Yellow Mustard Bottle that is to the upper right of the apple”.

TABLE VI: **ETRG-B** Real robot results on RGA spatial reasoning.

Methods	Grounding (%)	Grasp Succ. (%)
ETRG-B w/o depth (Ours)	85.0	70.0
ETRG-B	85.0	75.0

test scene, there are three identical object instances, and spatial language expression are used to specify the target. To increase the difficulty of spatial reasoning, we create test cases with four objects and seven objects. As illustrated in Table V, both the proposed methods, with and without depth fusion, demonstrate strong performance in handling complex spatial reasoning tasks. Our model with depth fusion achieves slightly higher performance compared to the RGB-only method.

Real Robot Results: We conducted experiments using a Franka Emika Panda robot equipped with a FESTO DHAS soft gripper. We collected over 10 household objects and created scenes with 6 randomly selected objects. Each scene included up to 3 duplicated instances of one category to test spatial reasoning. For each baseline, we report object grounding accuracy, which assesses whether the grasp is on the correct target, and the overall grasp success rate. A detailed visualization of correct mustard bottle identification with feasible grasp poses is shown in Fig. 4. Across 40 grasp attempts with different object arrangements (Table VI), both methods achieve comparable grounding performance, with our model incorporating depth information showing slightly better grasping accuracy.

V. CONCLUSION

In this work, we presented a novel CLIP-based parameter-efficient tuning framework that can be adapted to a range of tasks, including RES, RGS, and RGA tasks. Our method incorporated a vision-language fusion adapter and a depth-fusion branch, enabling effective open-vocabulary object grounding and robot grasping. We further explored the spatial reasoning capabilities in robot grasping, which the original CLIP [1] model does not address. The proposed models demonstrated competitive performance across these challenging vision language and robotics tasks. The current method may under-perform in highly cluttered scene.

REFERENCES

- [1] A. Radford, J. W. Kim, C. Hallacy, A. Ramesh, G. Goh, S. Agarwal, G. Sastry, A. Askell, P. Mishkin, J. Clark, *et al.*, “Learning transferable visual models from natural language supervision,” in *International conference on machine learning*. PMLR, 2021, pp. 8748–8763.
- [2] H. Yu, X. Lou, Y. Yang, and C. Choi, “Iosg: Image-driven object searching and grasping,” in *2023 IEEE/RSJ International Conference on Intelligent Robots and Systems (IROS)*. IEEE, 2023, pp. 3145–3152.
- [3] K. Xu, H. Yu, Q. Lai, Y. Wang, and R. Xiong, “Efficient learning of goal-oriented push-grasping synergy in clutter,” *IEEE Robotics and Automation Letters*, vol. 6, no. 4, pp. 6337–6344, 2021.
- [4] X. Lou, Y. Yang, and C. Choi, “Collision-aware target-driven object grasping in constrained environments,” in *2021 IEEE International Conference on Robotics and Automation (ICRA)*. IEEE, 2021, pp. 6364–6370.
- [5] X. Lou, H. Yu, R. Worobel, Y. Yang, and C. Choi, “Adversarial object rearrangement in constrained environments with heterogeneous graph neural networks,” in *2023 IEEE/RSJ International Conference on Intelligent Robots and Systems (IROS)*. IEEE, 2023, pp. 1008–1015.
- [6] M. Danielczuk, A. Kurenkov, A. Balakrishna, M. Matl, D. Wang, R. Martín-Martín, A. Garg, S. Savarese, and K. Goldberg, “Mechanical search: Multi-step retrieval of a target object occluded by clutter,” in *2019 International Conference on Robotics and Automation (ICRA)*. IEEE, 2019, pp. 1614–1621.
- [7] M. Oquab, T. Darcet, T. Moutakanni, H. Vo, M. Szafraniec, V. Khalidov, P. Fernandez, D. Haziza, F. Massa, A. El-Nouby, *et al.*, “Dinov2: Learning robust visual features without supervision,” *arXiv preprint arXiv:2304.07193*, 2023.
- [8] X. Chen and K. He, “Exploring simple siamese representation learning,” in *Proceedings of the IEEE/CVF conference on computer vision and pattern recognition*, 2021, pp. 15 750–15 758.
- [9] H. Yu and C. Choi, “Self-supervised interactive object segmentation through a singulation-and-grasping approach,” in *European Conference on Computer Vision*. Springer, 2022, pp. 621–637.
- [10] C. Xie, Y. Xiang, A. Mousavian, and D. Fox, “Unseen object instance segmentation for robotic environments,” *IEEE Transactions on Robotics*, pp. 1–17, 2021.
- [11] G. Tziafas, X. Yucheng, A. Goel, M. Kasaei, Z. Li, and H. Kasaei, “Language-guided robot grasping: Clip-based referring grasp synthesis in clutter,” in *7th Annual Conference on Robot Learning*, 2023.
- [12] Y. Yang, H. Yu, X. Lou, Y. Liu, and C. Choi, “Attribute-based robotic grasping with data-efficient adaptation,” *IEEE Transactions on Robotics*, 2024.
- [13] H. Ahn, O. Kwon, K. Kim, J. Jeong, H. Jun, H. Lee, D. Lee, and S. Oh, “Visually grounding language instruction for history-dependent manipulation,” in *2022 International Conference on Robotics and Automation (ICRA)*. IEEE, 2022, pp. 675–682.
- [14] K. Xu, S. Zhao, Z. Zhou, Z. Li, H. Pi, Y. Zhu, Y. Wang, and R. Xiong, “A joint modeling of vision-language-action for target-oriented grasping in clutter,” in *2023 IEEE International Conference on Robotics and Automation (ICRA)*. IEEE, 2023, pp. 11 597–11 604.
- [15] Y. Yang, Y. Liu, H. Liang, X. Lou, and C. Choi, “Attribute-based robotic grasping with one-grasp adaptation,” in *2021 IEEE International Conference on Robotics and Automation (ICRA)*. IEEE, 2021, pp. 6357–6363.
- [16] A. D. Vuong, M. N. Vu, B. Huang, N. Nguyen, H. Le, T. Vo, and A. Nguyen, “Language-driven grasp detection,” in *Proceedings of the IEEE/CVF Conference on Computer Vision and Pattern Recognition*, 2024, pp. 17902–17912.
- [17] T. Nguyen, M. N. Vu, B. Huang, A. Vuong, Q. Vuong, N. Le, T. Vo, and A. Nguyen, “Language-driven 6-dof grasp detection using negative prompt guidance,” in *ECCV*, 2024.
- [18] S. Huang, I. Ponomarenko, Z. Jiang, X. Li, X. Hu, P. Gao, H. Li, and H. Dong, “Manipvqa: Injecting robotic affordance and physically grounded information into multi-modal large language models,” *arXiv preprint arXiv:2403.11289*, 2024.
- [19] Y. Qian, X. Zhu, O. Biza, S. Jiang, L. Zhao, H. Huang, Y. Qi, and R. Platt, “Thinkgrasp: A vision-language system for strategic part grasping in clutter,” *arXiv preprint arXiv:2407.11298*, 2024.
- [20] S. Jin, J. Xu, Y. Lei, and L. Zhang, “Reasoning grasping via multi-modal large language model,” *arXiv preprint arXiv:2402.06798*, 2024.
- [21] J. Kirkpatrick, R. Pascanu, N. Rabinowitz, J. Veness, G. Desjardins, A. A. Rusu, K. Milan, J. Quan, T. Ramalho, A. Grabska-Barwinska, *et al.*, “Overcoming catastrophic forgetting in neural networks,” *Proceedings of the national academy of sciences*, vol. 114, no. 13, pp. 3521–3526, 2017.
- [22] Z. Xu, Z. Chen, Y. Zhang, Y. Song, X. Wan, and G. Li, “Bridging vision and language encoders: Parameter-efficient tuning for referring image segmentation,” in *Proceedings of the IEEE/CVF International Conference on Computer Vision*, 2023, pp. 17 503–17 512.
- [23] Y. Wang, J. Li, X. Zhang, B. Shi, C. Li, W. Dai, H. Xiong, and Q. Tian, “Barleria: An efficient tuning framework for referring image segmentation,” in *The Twelfth International Conference on Learning Representations*.
- [24] R. Hu, M. Rohrbach, and T. Darrell, “Segmentation from natural language expressions,” in *Computer Vision—ECCV 2016: 14th European Conference, Amsterdam, The Netherlands, October 11–14, 2016, Proceedings, Part I 14*. Springer, 2016, pp. 108–124.
- [25] Q. Sun, H. Lin, Y. Fu, and X. Xue, “Language guided robotic grasping with fine-grained instructions,” in *2023 IEEE/RSJ International Conference on Intelligent Robots and Systems (IROS)*. IEEE, 2023, pp. 1319–1326.
- [26] Z. Wang, Y. Lu, Q. Li, X. Tao, Y. Guo, M. Gong, and T. Liu, “Cris: Clip-driven referring image segmentation,” in *Proceedings of the IEEE/CVF conference on computer vision and pattern recognition*, 2022, pp. 11 686–11 695.
- [27] Y. Yan, X. He, W. Wang, S. Chen, and J. Liu, “Eavl: Explicitly align vision and language for referring image segmentation,” *arXiv preprint arXiv:2308.09779*, 2023.
- [28] Y. Lu, Y. Fan, B. Deng, F. Liu, Y. Li, and S. Wang, “Vl-grasp: a 6-dof interactive grasp policy for language-oriented objects in cluttered indoor scenes,” in *2023 IEEE/RSJ International Conference on Intelligent Robots and Systems (IROS)*. IEEE, 2023, pp. 976–983.
- [29] C. Tang, D. Huang, L. Meng, W. Liu, and H. Zhang, “Task-oriented grasp prediction with visual-language inputs,” in *2023 IEEE/RSJ International Conference on Intelligent Robots and Systems (IROS)*. IEEE, 2023, pp. 4881–4888.
- [30] C. Cheang, H. Lin, Y. Fu, and X. Xue, “Learning 6-dof object poses to grasp category-level objects by language instructions,” in *2022 International Conference on Robotics and Automation (ICRA)*. IEEE, 2022, pp. 8476–8482.
- [31] M. Shridhar, L. Manuelli, and D. Fox, “Cliport: What and where pathways for robotic manipulation,” in *Conference on robot learning*. PMLR, 2022, pp. 894–906.
- [32] N. Houlisby, A. Giurgiu, S. Jastrzebski, B. Morrone, Q. De Laroussilhe, A. Gesmundo, M. Attariyan, and S. Gelly, “Parameter-efficient transfer learning for nlp,” in *International conference on machine learning*. PMLR, 2019, pp. 2790–2799.
- [33] S. Chen, C. Ge, Z. Tong, J. Wang, Y. Song, J. Wang, and P. Luo, “Adaptformer: Adapting vision transformers for scalable visual recognition,” *Advances in Neural Information Processing Systems*, vol. 35, pp. 16 664–16 678, 2022.
- [34] S. Jie and Z.-H. Deng, “Convolutional bypasses are better vision transformer adapters,” *arXiv preprint arXiv:2207.07039*, 2022.
- [35] X. L. Li and P. Liang, “Prefix-tuning: Optimizing continuous prompts for generation,” *arXiv preprint arXiv:2101.00190*, 2021.
- [36] E. J. Hu, Y. Shen, P. Wallis, Z. Allen-Zhu, Y. Li, S. Wang, L. Wang, and W. Chen, “Lora: Low-rank adaptation of large language models,” *arXiv preprint arXiv:2106.09685*, 2021.
- [37] K. Zhou, J. Yang, C. C. Loy, and Z. Liu, “Learning to prompt for vision-language models,” *International Journal of Computer Vision*, vol. 130, no. 9, pp. 2337–2348, 2022.
- [38] K. He, X. Zhang, S. Ren, and J. Sun, “Deep residual learning for image recognition,” in *CVPR*, 2016, pp. 770–778.
- [39] A. Dosovitskiy, “An image is worth 16x16 words: Transformers for image recognition at scale,” *arXiv preprint arXiv:2010.11929*, 2020.
- [40] A. Vaswani, “Attention is all you need,” *Advances in Neural Information Processing Systems*, 2017.
- [41] B. Chen, Z. Hu, Z. Ji, J. Bai, and W. Zuo, “Position-aware contrastive alignment for referring image segmentation,” *arXiv preprint arXiv:2212.13419*, 2022.
- [42] H. Ding, C. Liu, S. Wang, and X. Jiang, “Vision-language transformer and query generation for referring segmentation,” in *Proceedings of the IEEE/CVF International Conference on Computer Vision*, 2021, pp. 16 321–16 330.

- [43] L. Yu, Z. Lin, X. Shen, J. Yang, X. Lu, M. Bansal, and T. L. Berg, "Mattnet: Modular attention network for referring expression comprehension," in *Proceedings of the IEEE conference on computer vision and pattern recognition*, 2018, pp. 1307–1315.
- [44] G. Luo, Y. Zhou, R. Ji, X. Sun, J. Su, C.-W. Lin, and Q. Tian, "Cascade grouped attention network for referring expression segmentation," in *Proceedings of the 28th ACM International Conference on Multimedia*, 2020, pp. 1274–1282.
- [45] Y. Hu, Q. Wang, W. Shao, E. Xie, Z. Li, J. Han, and P. Luo, "Beyond one-to-one: Rethinking the referring image segmentation," in *Proceedings of the IEEE/CVF International Conference on Computer Vision*, 2023, pp. 4067–4077.
- [46] N. Kim, D. Kim, C. Lan, W. Zeng, and S. Kwak, "Restr: Convolution-free referring image segmentation using transformers," in *Proceedings of the IEEE/CVF Conference on Computer Vision and Pattern Recognition*, 2022, pp. 18 145–18 154.
- [47] S. Kazemzadeh, V. Ordonez, M. Matten, and T. Berg, "Referitgame: Referring to objects in photographs of natural scenes," in *Proceedings of the 2014 conference on empirical methods in natural language processing (EMNLP)*, 2014, pp. 787–798.
- [48] J. Mao, J. Huang, A. Toshev, O. Camburu, A. L. Yuille, and K. Murphy, "Generation and comprehension of unambiguous object descriptions," in *Proceedings of the IEEE conference on computer vision and pattern recognition*, 2016, pp. 11–20.
- [49] V. K. Nagaraja, V. I. Morariu, and L. S. Davis, "Modeling context between objects for referring expression understanding," in *Computer Vision–ECCV 2016: 14th European Conference, Amsterdam, The Netherlands, October 11–14, 2016, Proceedings, Part IV 14*. Springer, 2016, pp. 792–807.
- [50] Z. Yang, J. Wang, Y. Tang, K. Chen, H. Zhao, and P. H. Torr, "Lavt: Language-aware vision transformer for referring image segmentation," in *Proceedings of the IEEE/CVF Conference on Computer Vision and Pattern Recognition*, 2022, pp. 18 155–18 165.
- [51] A. Depierre, E. Dellandréa, and L. Chen, "Jacquard: A large scale dataset for robotic grasp detection," in *2018 IEEE/RSJ International Conference on Intelligent Robots and Systems (IROS)*. IEEE, 2018, pp. 3511–3516.
- [52] E. Rohmer, S. P. N. Singh, and M. Freese, "V-rep: A versatile and scalable robot simulation framework," in *2013 IEEE/RSJ International Conference on Intelligent Robots and Systems*, 2013, pp. 1321–1326.
- [53] B. Calli, A. Singh, A. Walsman, S. Srinivasa, P. Abbeel, and A. M. Dollar, "The ycb object and model set: Towards common benchmarks for manipulation research," in *2015 international conference on advanced robotics (ICAR)*. IEEE, 2015, pp. 510–517.